JACS
JOURNAL OF THE AMERICAN CHEMICAL SOCIETY
Article
pubs.acs.org/JACS

DNA Switches on the Two-Photon Efficiency of an Ultrabright Triphenylamine Fluorescent Probe Specific of AT Regions

Blaise Dumat,[†,∥] Guillaume Bordeau,[†,§,∥] Elodie Faurel-Paul,[†] Florence Mahuteau-Betzer,[†] Nicolas Saettel,[†] Germain Metge,[‡] Céline Fiorini-Debuisschert,[‡] Fabrice Charra,[‡] and Marie-Paule Teulade-Fichou*[,†]

[†]Institut Curie, CNRS UMR-176, Centre Universitaire d'Orsay, Paris-Sud 91405 Orsay Cedex France
[‡]CEA- Saclay, DSM-IRAMIS/SPCSI/Laboratoire NanoPhotonique, 91191 Gif-sur-Yvette, France

Supporting Information

ABSTRACT: We report on the design and synthesis of two-photon fluorescent triphenylamines bearing two or three vinyl branches terminated by a *N*-methyl benzimidazolium moiety. The new compounds (TP-2Bzim, TP-3Bzim) are light-up fluorescent DNA probes with a long wavelength emission (>580 nm). Compared to their pyridinium models, the TP-Bzim dyes exhibit a remarkable improvement of both their DNA affinity and fluorescence quantum yield, especially for the two-branch derivative (TP-2Bzim: Φ_F = 0.54, K_a = 10^7 M^{-1}), resulting in a large fluorescence emission turn-on ratio of up to 140. Concomitantly, the two-photon absorption cross-section of TP-2Bzim is dramatically enhanced upon DNA binding (δ = 1080 vs 110 GM for the free form). This effect of the DNA matrix on the nonlinear absorption is uncovered for the first time. This is attributed to a tight fit of the molecule inside the minor groove of AT-rich DNA which induces geometrical rearrangements in the dye ground state as supported by circular dichroism and molecular modeling data. Consequently, TP-2bzim displays an exceptional two-photon molecular brightness ($\delta \times \Phi_F$ = 583 GM), a value unrivalled for a small biofluorophore. These properties enable to image nuclear DNA in fixed cells at submicromolar concentration ([TP-2Bzim] = 100 nM) and to visualize ultrabright foci of centromeric AT-rich chromatin. Finally TP-2Bzim exhibits a high photostability, is live-cell permeant, and does not require RNase treatment. This outstanding combination of optical and biological properties makes TP-2Bzim a bioprobe surpassing the best DNA stainers and paves the way for studying further nonlinear optical processes in DNA.

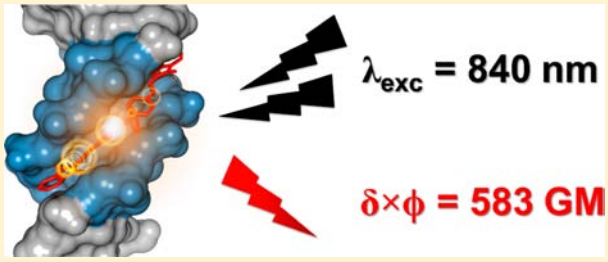

INTRODUCTION

Fluorescent probes have become invaluable tools in cell biology and medical imaging, and new fluorescent reporters, spanning from small organic dyes[1,2] to inorganic nanocrystals (quantum dots)[3] and fluorescent proteins (FPs),[4] are continuously proposed by industrial and academic research, while considerable efforts are concomitantly made to develop new ultrasensitive instrumentation.[5] These two research domains are tightly intertwined as the rapid evolution of optical microscopy techniques is calling constantly for new dyes with optimized optical properties to fulfill the promise of increased temporal and spatial resolutions.[6,7]

The emergence in the 1990s of two-photon laser scanning microscopy[8−10] has been one of the most prominent amelioration in fluorescence imaging, allowing the development of in-depth[11−13] and/or intravital[14−16] tissue imaging. In this technique, excitation is induced by the simultaneous absorption of two photons with half the energy required for the corresponding one photon absorption process. Therefore, the excitation wavelength is in the near-infrared (NIR) range (700−1000 nm) where the absorption and diffusion of light by biological samples is minimized thereby allowing deep tissue imaging (up to 1 mm). Moreover, the two-photon excitation is limited to a small femtoliter volume at the focal point of the laser resulting in an intrinsic 3D image resolution and a limited irradiation of the sample. A high density of photons is required to enable simultaneous absorption of two photons, and excitation is usually performed using femtosecond lasers. Despite the lower energy of the IR light compared to the visible light, this excitation mode has been proven to induce damages to the samples and bleaching of the dyes, especially when using classical fluorophores that display generally low two-photon absorption (2PA) capacities.[17] Thus the laser power has to be kept as low as possible to avoid too high peak powers in the excitation volume, which may result in modest imaging performances. Hence, there is a strong need of dedicated fluorophores with a high two-photon absorption cross-section to exploit the full potential of two-photon laser scanning microscopy, in particular for fluorescence lifetime imaging (FLIM) and intravital imaging. Over the past decades, considerable efforts have been carried out to provide new dyes

Received: May 14, 2013
Published: August 5, 2013

   dx.doi.org/10.1021/ja404422z | J. Am. Chem. Soc. 2013, 135, 12697−12706

with optimized two-photon absorption cross-sections (δ),[13,18−22] but due to the difficulty to find the right balance between the optical properties and the biological constraints, the challenge remains quite topical.

Indeed, when selecting the appropriate 2PA dye for fluorescence imaging, many factors should be considered depending on the application. In particular, certain photophysical and chemical characteristics will be of prime importance: these include (i) a high 2PA molecular brightness (i.e., product of 2PA absorption cross-section and quantum yield = $\delta \cdot \Phi_F$ also called action cross-section) to improve the signal-to-noise (S/N) ratio thus enabling low dye loading and reduced laser power; (ii) a high photochemical stability, which is crucial to follow processes on a long time scale; and (iii) a NIR/long wavelength emission to avoid overlap with fluorescence of endogeneous cell components and to improve collection of the emitted light in thick sample. These basic characteristics, although prerequisite, are hardly simultaneously fulfilled by the same molecular agent. Additionally, biological criteria, such as water solubility cell permeation, low toxicity, specific affinity for a given cell type or cellular compartment, come into play thus adding to the difficulty and making the design of "the ideal 2PA dye" highly demanding. More specifically, in the class of DNA imaging probes, most commercial dyes have low 2PA absorption (δ values from 5 GM to <50 GM).[23,24] In addition, the red emitting dyes like TO-PRO cyanines or propidium iodide (PI) have inherent drawbacks, such as very fast bleaching for the former and poor cell permeation and poor DNA vs RNA specificity for the latter. Imaging of DNA is thus essentially performed with blue-emitting dyes (DAPI and Hoechst compounds) which are more resistant but require either harmful short-wavelength excitation that is cytotoxic *per se* or huge two-photon excitation intensities, also leading to cell damages. Overall, there is a lack of a ubiquitous 2PA DNA probe with a long wavelength/NIR emission displaying a satisfying combination of the above-mentioned criteria and therefore usable for cellular imaging in various circumstances.

In our ongoing research on nucleic acid probes,[25−27] we have shown recently that π-conjugated triphenylamines (TP), typical 2PA materials, may behave as DNA-specific long wavelength/NIR fluorescent emitters provided that a cationic acceptor is linked at the TP branch termini.[28] This study has led to the emergence of vinyl TPs as biocompatible labels,[29] while this chemical class was confined so far to model systems[30,31] and material applications.[32−34]This first generation of vinyl triphenylamines was based on the introduction of pyridinium acceptors tethered to the central triphenylamine donor via vinyl arms which resulted in the classical V-shaped and octupolar (TP-2Py, TP-3Py) arrangements (Figure 1).[30,31,35,36] These compounds were shown to display high two-photon absorption cross-sections (from 200 to 700 GM at 800 nm) and in addition are nonfluorescent in water whereas featuring a long wavelength red emission (650 nm < λ_{max} < 680 nm) upon binding to DNA.[28] However, this first series exhibits modest fluorescence quantum yields in DNA (0.07 and 0.01 for TP-2Py and TP-3Py, respectively), leading to low brightness which could severely limit the scope of their application for staining nuclear DNA or oligonucleotides. We thus speculated that exploring the chemical space around the triphenylamine core should enable optimization of the optical properties of this chemical class.

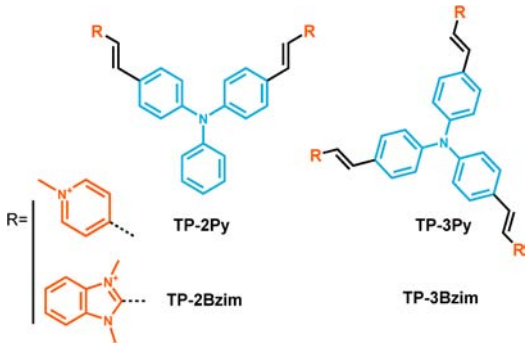

Figure 1. General structure of the TP-Py and TP-Bzim dyes.

We show herein that the introduction of a more extended π-deficient heterocyclic system, i.e., *N*-methyl benzimidazolium moiety, in place of the pyridinium unit results in strong and concomitant optimization of both optical performances and DNA binding parameters. Consequently, this led to the identification of a new 2PA probe called TP-2Bzim (Figure 1) that possesses an unprecedented two-photon molecular brightness inside DNA combined with high affinity and exquisite selectivity for AT-rich DNA regions. Importantly we show that the DNA matrix has a dramatic influence not only on fluorescence emission but also on the two photon absorption. Moreover the new TP-2Bzim dye is easily accessible on a large preparative scale, possesses exceptional photostability under one- and two-photon excitation, is live cell permeant, and consequently fulfills the above-mentioned characteristics making it an outstanding fluorescent DNA 2PA probe.

RESULTS AND DISCUSION

Design and Synthesis. Inspired by the well-established molecular guidelines in the design of 2PA molecular systems, we turned our attention toward the use of π-deficient heterocyclic systems, such as benzothiazole and benzimidazole.[37,38] These motifs can be, in principle, easily methylated which will afford the cationic charge inducing DNA binding and should reinforce the internal charge transfer. However, in our hands the benzothiazolium motif once branched on the TP core appeared rapidly unstable in water where spontaneous demethylation occurred.[39] Therefore we focused our attention on the *N*-methyl benzimidazolium series, which resulted in the preparation of the two compounds TP-2Bzim and TP-3Bzim achieved through a simple Wittig reaction between the bis- and tris-formyl triphenylamine (**3a**,**b**) and the (*N*-methyl benzimidazole)-methyltriphenylphosphonium chloride **2** (Scheme 1).

This method is more economical and easier to achieve than the Heck reaction previously used for the pyridinium derivatives.[28] The phosphonium chloride **2** was readily prepared in two steps by condensation of *N*-methyl-1,2-benzenediamine and chloroacetic acid, followed by nucleophilic substitution of the chlorine by triphenylphosphine (64% overall yield). Reaction of **2** with **3a**,**b** in methanol in the presence of sodium methanolate led to the neutral intermediates with good yields (65−85%), and subsequent methylation afforded TP-2Bzim and TP-3Bzim in 55% and 86% yields, respectively. As expected from the Wittig reaction only the *E* conformation was obtained.

The two TP-Bzim compounds are dark-red powders, displaying high water solubility. Of note the compounds obey Beer's law over a wide concentration range (up to 100 μM,

Scheme 1. Synthesis of the TP-Bzim Derivatives

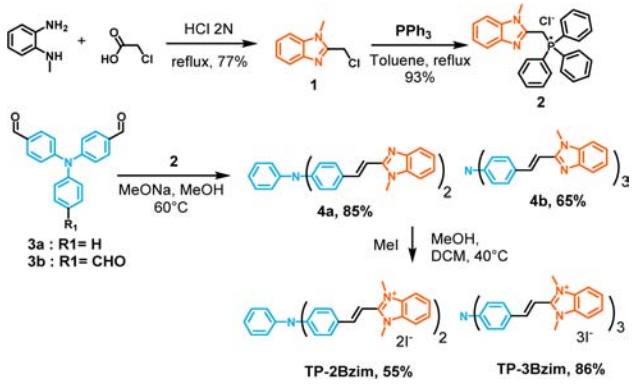

Figure S1) indicating that they do not aggregate in aqueous media.

Light-Up Fluorescence in DNA. The one-photon absorption and emission properties of the new TP-Bzim compounds were characterized in glycerol and in a buffered aqueous solution (pH 7.2) with and without DNA. In our previous studies,[28,40] we observed that both absorption and fluorescence can be somewhat influenced by the nature and the origin of the double stranded DNA (native polymers, synthetic oligomers). To simplify the measurements of affinity constants and understand more thoroughly the sequence selectivity of the TP dyes, we studied them in presence of two custom-made self-complementary duplex oligonucleotides of variable sequence and length: DrewAT, a 14bp duplex with a 6AT central core, previously used as a model of duplex AT-rich DNA[41] and ds26, a 26bp duplex with mixed AT/GC content[42] (see base sequences in the Material and Methods section).

As expected, the TP-Bzim dyes exhibit high molecular absorption coefficients (Table 1) with absorption maxima strongly blue-shifted (~52−58 nm) as compared to the TP-Py series, which may reveal a lower degree of conjugation of the Bzim branches originating in their lower planarity (*vide infra*).

Table 1. Linear Optical Properties of the New Series TP-Bzim and of the Reference Compounds TP-Py in pH 7.2 Cacodylate Buffer, Glycerol, and DrewAT[a]

		$\lambda_{abs}/\lambda_{em}$	ε	$\Delta\lambda$	Φ_F
	buffer	474/650	39 900	176	<0.005
TP-2Py	glycerol	496/649	37 400	153	0.11
	DrewAT	509/656	31 400	147	0.07
	buffer	474/684	59 000	210	<0.005
TP-3Py	glycerol	492/666	66 000	174	0.13
	DrewAT	499/684	51 000	185	0.01
	buffer	432/620	42 500	188	<0.005
TP-2Bzim	glycerol	448/602	40 400	154	0.35
	DrewAT	476/585	44 400	109	0.54
	buffer	430/640	68 900	210	<0.05
TP-3Bzim	glycerol	440/604	57 200	164	0.42
	DrewAT	468/591	62 400	123	0.34

[a] λ_{abs}: maximum absorption wavelength (nm); λ_{em}: maximum emission wavelength (nm); ε: molar absorption coefficient ($mol^{-1}\cdot L\cdot cm^{-1}$); $\Delta\lambda$: Stokes's shift expressed in nm; Φ_F: fluorescence quantum yields were measured using rhodamine 101 in ethanol as reference. Cacodylate buffer: 10 mM sodium cacodylate buffer (pH 7.2, 100 mM NaCl). DrewAT: 10 mol equiv of DrewAT.

Titration of TP-Bzim compounds by DrewAT induces significant red-shift of the absorption ($\Delta\lambda_{max}$ = 20−45 nm) with a neat isosbestic point in the case of TP-2Bzim indicating the formation of at least one ligand/DNA complex species (Figures 2A and S2). In the meantime, the fluorescence signal

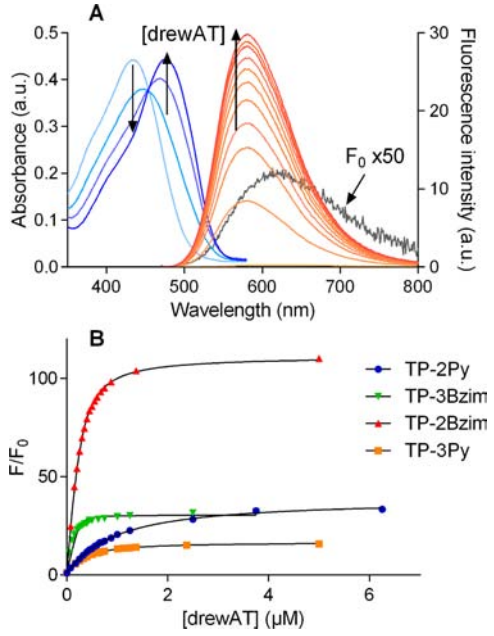

Figure 2. (A) Absorption and fluorescence spectra of TP-2Bzim (at 10 and 0.25 μM, respectively) upon addition of DrewAT in sodium cacodylate buffer 10 mM pH 7.2, NaCl 400 mM. (B) Titration curves obtained by plotting the fluorescence enhancement F/F_0 as function of Drew AT concentration (F = integrated fluorescence intensity of the complex, F_0 = fluorescence of the free dye), [drewAT] is expressed in molar concentration (i.e., per duplex).

is restored with a pronounced fluorescence enhancement and a significant blue-shift of the emission wavelength in DNA with regard to buffer (35−50 nm, Figures 2A and S2). The same trend is observed in glycerol, meaning that the Bzim dyes are rather responsive to the constraints of the environment (viscosity/DNA interaction). Most remarkably, the amplitude of the fluorescence increase is dramatically larger for the new dyes in particular for TP-2Bzim (F_{max}/F_0 of 140 vs 24 for TP-2Py). Calculation of quantum yields indicates very high values (Φ_F/TP-2Bzim = 0.54; Φ_F/TP-3 Bzim = 0. 34) thereby representing a 6−34-fold increase as compared to the pyridinium counterparts (Table 1). This remarkable improvement of Φ_F is also apparent in glycerol albeit more modest (3-fold increase), suggesting that this effect lies not only in the chemical characteristics of the benzimidazolium group (increased rigidity, increased number of π-electrons) but also in a more favorable interaction with the DNA matrix. The influence of DNA is particularly striking when considering the number of branches. In glycerol, the quantum yields are quite similar for the two- and three-branch analogs in both series, respectively. This is consistent with the observation that for V-shaped and octupolar molecules the emitting state seems to be localized on a single branch, yielding similar quantum yields irrespective of the number of branches.[30] In presence of DNA however, the photophysics of the excited state is clearly modified, since the two-branch compounds exhibit significantly higher quantum efficiency than their three-branch counterparts. Moreover, the

dx.doi.org/10.1021/ja404422z | J. Am. Chem. Soc. 2013, 135, 12697−12706

quantum yield of TP-2Bzim is further increased when shifting from glycerol to DNA (0.34 vs 0.54), whereas it is decreased for the three other compounds pointing to the influence of specific dye/DNA interactions.

The light-up effect of DNA on the fluorescence of TP-dyes is attributable to several processes: the emission of the free dyes is likely quenched by vibrations and rotations around the double bond and around the central nitrogen atom as the scaffold is rather flexible. On the other hand the interaction with water molecules of highly polar excited states is known to deactivate the radiative pathway. Consequently, the strong emission enhancement of TP-dyes upon DNA binding is likely the result of two contributions: restriction of intramolecular rotations of the excited state through immobilization inside the DNA matrix and water desolvation. In addition, conformational changes induced by DNA binding can also be involved.

DNA Structure Selectivity. To gain insight into the structure preference of the TP compounds, we evaluated the ability of various nucleic acid matrices to restore the dye fluorescence. Thus a 17-mer DNA single strand (ssDNA) and total calf liver RNA (cl-RNA) that contains a wide variety of secondary structures were added to the duplex oligonucleotide set.

Remarkably, TP-2Bzim shows a strong and selective fluorescence enhancement in the presence of duplex DNA (F_{max}/F_0 = 140, Figure 3 and Table S1), whereas RNA and

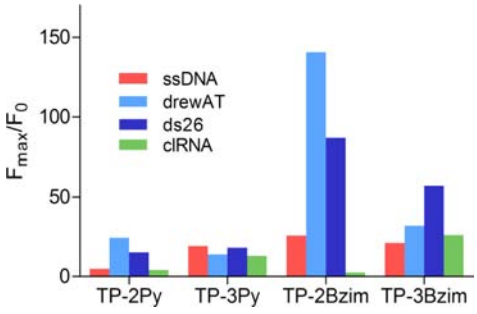

Figure 3. Maximum enhancement of the fluorescence signal of TP-dyes in presence of various forms of nucleic acids in saturation conditions, [TP dye] = 1 μM, cacodylate buffer pH 7.2, 400 mM NaCl, DNA 10−20 molar equiv, see sequences in the Material and Methods section.

ssDNA induce a dramatically lower response (F_{max}/F_0 = 2 and 25, respectively, Table S1). In addition the dye exhibits a clear preference for the AT-rich duplex as compared to ds26 (F_{max}/F_0 = 86). The same trend is observed with the original TP-2Py but with a considerably lower intensity (F_{max}/F_0 = 24 for Drew AT and see Table S1). Finally, the three-branch analogues of both series (TP-3Bzim, TP-3Py) display a much less discriminating behavior that might be attributable to their triscationic charge favoring nonspecific electrostatic-driven association with any polyanionic matrix. The fluorescence enhancement factor F_{max}/F_0 is a semiquantitative indicator of selectivity and thus represents a key parameter for high contrast imaging in view of fluorescence microscopy applications. In this regard TP-2Bzim appears the best candidate for staining duplex DNA, as its strong and preferential fluorescence response should result in high brightness and excellent imaging contrast.

However, one should not expect a systematic correlation between the fluorescence enhancement and the DNA affinity, thus to further rationalize the TP-dye/DNA interaction binding constants (K_a) were determined from the fluorimetric titrations using nonlinear curve fitting analysis (Figures 2B and S3−S4). In most cases, with the exception of TP-3Bzim, the 1:1 stoichiometry model fitted the experimental data with excellent correlation coefficients (Table S2). Remarkably, the highest K_a value (1.2×10^7 M^{-1}) was obtained for TP-2Bzim in Drew AT and is 1 order of magnitude larger than that obtained for TP-2Py ($K_a = 1.2 \times 10^6$ M^{-1}) in the same duplex. Significantly lower K_a were determined in ds26, and this trend is particularly striking for TP-2Bzim [K_a(DrewAT)/K_a(ds26) = 12], while a factor of 3.5 is observed for TP-2Py (Table S1). These data are fully consistent with the fluorescence response confirming the pronounced preference of TP-2Bzim for AT-rich DNA. Although drewAT has been previously used as a model for AT-rich DNA, it also contains two GC-tracts, so to unambiguously confirm the AT preference of the dye, we performed experiments in presence of the polynucleotides poly(dA-dT)$_2$ and poly(dG-dC)$_2$ (Figure S5). The increase in fluorescence of TP-2Bzim in the former is remarkably high and similar to that observed in DrewAT (F/F_0 = 140), while it is very low in presence of the latter (F/F_0 < 15−10). In addition in this case the binding is very sluggish as judged by the shape of the curve that does not display saturation.

Globally the three-branch derivatives exhibit DNA affinities increased by a factor of 2−3 as compared to their two-branch counterparts (Table S1). However, the curves could not be fitted properly with the 1:1 model especially in the case of TP-3Bzim and DrewAT (Figure S3, Table S2). As the sharp profile of the curve is indicative of a strong binding, the K_a was assumed to be >10^7 M^{-1} but not measurable in our conditions. Obviously TP-3Py and TP-3Bzim feature a three-bladed propeller topology *a priori* less prone to interact in a well-defined manner with the double B-helix structure as compared to their two-branch analogues, and contribution of secondary sites and/or nonspecific electrostatic interactions cannot be excluded albeit these are minimized by the high-salt conditions (400 mM NaCl, Figures S3−4) used on this purpose. Nonetheless the AT preference of TP-3Bzim, although less clear from titrations with oligonucleotides, was also evidenced by the experiments with homopolynucleotides (Figure S5).

TP-2Bzim, a perfect match in the groove. Based on the nonplanar twisted V-shape of the two-branch molecules and their apparent preference for AT-sequences, the TP dyes were assumed to interact with duplex DNA via insertion in the minor groove.[43−45] To support this hypothesis, circular dichroism (CD) experiments were conducted (Figure 4). Upon addition of increasing amounts of TP-2Bzim to a solution of Drew AT, a strong induced CD (ICD) signal in the dye absorption band was observed. ICD signal was substantially the same with TP-3Bzim but with a slightly lower intensity, and the same behavior is observed with the TP-Py series (Figure S6). Strong and positive ICD in the ligand absorption band is a characteristic feature of DNA minor groove binders. On the other hand, intercalation between base pairs is usually accompanied by weak negative ICD signals.[46,47] Moreover the CD signal in the DNA absorption region (around 260 nm) remains unchanged upon addition of the TP derivatives, which is again consistent with minor-groove binding as this mode is known to affect poorly the DNA structure contrary to intercalation between bases.

More intriguingly, the interaction is featuring a bisignate (negative/positive) ICD signal. This is frequently associated to interchromophoric interactions reflecting excitonic coupling in

dx.doi.org/10.1021/ja404422z | J. Am. Chem. Soc. 2013, 135, 12697−12706

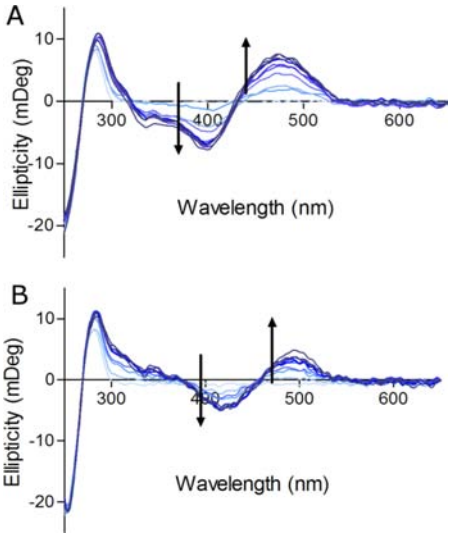

Figure 4. CD spectra of drewAT (10 μM) upon addition of TP-2Bzim and TP-3Bzim (0−10 mol equiv) in 10 mM sodium cacodylate buffer pH 7.2, 100 mM NaCl.

dimers formed by nearby chromophores in the groove or at the surface of the DNA.[48] However, the triphenylamine scaffold owing to its propeller shape is not prone to form dimers; as well this situation is not consistent with the 1:1 stoichoimetry inferred from the fluorimetric titrations. Therefore we hypothesize that the bisignate ICD signal is reflecting the positioning of two branches lying in the groove in a twisted geometry thereby mimicking a dimeric arrangement between adjacent chromophores. Each branch may thus behave like a single dipole resulting in excitonic coupling between the 2 branches.

On the basis of the data obtained by CD, we conducted molecular modeling calculations.

The docking results obtained in DrewAT (Figure 5) indicate that the complex formed either by the two- or three-armed TP is based on the insertion of two branches into the minor groove. The two-branch moiety adopts a volume and shape which fit snugly into the minor groove, occupying a 5−6 AT bp site (Figure 5A). This binding site size is consistent with the stronger binding affinity for DrewAT that features a central

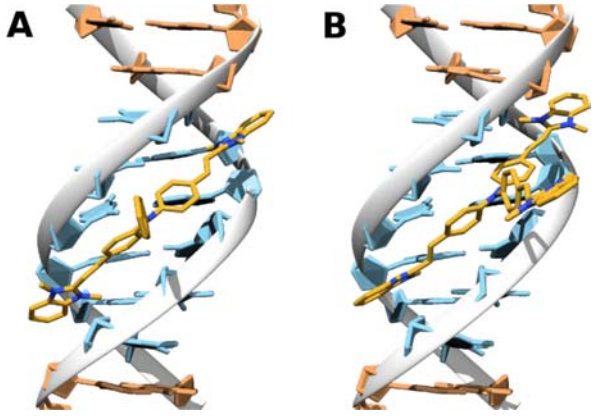

Figure 5. Models obtained after molecular modeling for the interaction of TP-2Bzim (A) and TP-3Bzim (B) with duplex DrewAT (AT bases in pale blue). Side view and models obtained for TP-Py compounds are shown in Figure S7.

6AT tract, whereas ds26 has a mixed sequence with only a 4AT site. This model emphasizes the flexibility of the triphenylamine core that adopts a slightly twisted V-shaped conformation, enabling perfect geometric match with the groove curvature and thereby optimization of the interactions. Interestingly in the case of TP-3Bzim, the position inside the DNA is very similar, while the third branch is sticking out of the helix without direct contact with the DNA matrix (Figure 5B). This demonstrates that the third branch is not immobilized and furthermore is in contact with the aqueous solvent, which is consistent with the lower quantum yield observed for TP-3Bzim. Furthermore this indicates that the DNA recognition motif is constituted by only two branches of the TP scaffold. The same holds for the TP-Py compounds (Figure S7). Finally, this observation provides a clue to understand the higher binding affinity measured for the three-branch scaffolds as the latter offer three binding motifs as compared to one for the two-branched scaffold, which may confer a gain in the binding entropy (Table S1).

Several contributions are involved in the binding of small molecules in the AT-rich minor groove, the complex formation being driven by hydrophobic, van der Waals, electrostatic, and H-bonding components.[49] The preference of ligands for AT-rich groove is commonly attributed to the smaller groove width of AT tracts and to steric repulsion induced by the guanine NH_2 in GC tracts. In addition the AT minor grooves display a more negative electrostatic potential as compared to other sequences, which is favorable to cation trapping. More recently the role of the spine of hydration in AT grooves has been documented.[50] The highly ordered water molecules present in the grooves could either mediate the interaction via H-bonding between the two partners[51,52] and/or create an important entropic gain when they are displaced out in the bulk solvent. In that sense enhanced hydrophobicity of the ligand and H-bonding capacity are recognized to be advantageous. In the present case both the Py and Bzim series do not present H-bonding donor sites, and thus the other contributions should be prominent. The larger aromatic surface of the Bzim motif as compared to the Py motif may result in enhanced hydrophobic effect and optimized van der Waals contacts with the walls of the grooves. This is furthermore supported by the significantly larger size of TP-2Bzim as compared to TP-2Py (Figures 5 and S7).[53] Moreover, due to the symmetry of the Bzim motif, the cationic charge is distributed on the two *N*-methyl ring nitrogens, while it is localized on one nitrogen atom in the Py motif (Figure S8). This difference in the spatial localization of the charge may significantly influence the interaction with the anionic phosphate backbone.

In conclusion, the modeling studies indicate a perfect geometric match between the TP-2Bzim compound and the AT minor groove which is made possible by the adaptability/flexibility of the two-branch scaffold. This tight fit inside DNA and the associated conformational changes are likely to impact the nonlinear optic (NLO) response in DNA.

NLO Properties: Influence of the DNA Matrix. The two-photon absorption spectra of the TP derivatives were measured in presence of DrewAT by two-photon excited fluorescence (Figure 6).

The shape of the 2PA spectra are almost identical for the four compounds with maximum intensity peaking at 840 nm in contrast to their one photon absorption spectra that are significantly blue-shifted for TP-Bzim compounds compared to TP-Py compounds (Figure S9). Remarkably all four com-

dx.doi.org/10.1021/ja404422z | J. Am. Chem. Soc. 2013, 135, 12697−12706

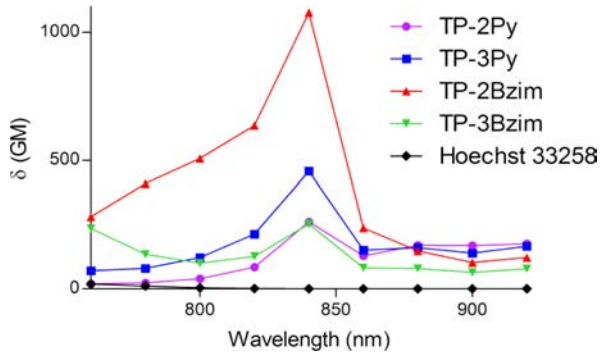

Figure 6. Nonlinear absorption spectra of the TP-dyes in presence of 10 mol equiv of DrewAT, 10 mM sodium cacodylate sodium buffer pH 7.2, 100 mM NaCl.

pounds show a high nonlinear response with two-photon absorption cross-section values (δ) ranging from 250 to 1080 GM (Table 2). The particularly high 2PA cross-section value of the TP-2Bzim is worth noting, in particular as compared to that of the three other compounds.

Table 2. NLO Properties of the TP Derivatives and Hoechst 33258 in Presence of DrewAT[a]

	$\lambda_{2PA}{}^{max}$ (nm)	δ (GM)	$\delta\times\Phi_F$ (GM)
TP-2Py	840	260	18
TP-3Py	840	460	5
TP-2Bzim	840	1080	583
TP-3Bzim	840	250	85
Hoechst 33258	760	19	7

[a] δ: two-photon absorption cross-section (GM), $\lambda_{2PA}{}^{max}$: maximum two-photon absorption wavelength (nm), $\delta\times\Phi_F$: two-photon action cross-section. The values of the fluorescence quantum yields are those of Table 1.Conditions: 10 mM sodium cacodylate buffer pH 7.2, 100 mM NaCl, 10 mol.equivalents of DrewAT.

Pioneering studies on triphenylamine derivatives demonstrated the role of dimensionality and hence of the number of branches on the 2PA performances. In this line octupolar arrangements are expected to have a much higher two-photon absorption cross-section than their V-shaped or quadrupolar analogs.[31,54] This structure−property relationship is verified in the TP-Py series and is consistent with our previous results obtained in calf thymus DNA.[28] Unexpectedly in the TP-Bzim series the opposite situation is observed, as the 2PA cross-section of TP-2Bzim is four times higher than that of TP-3Bzim. This striking difference points to the influence of the DNA environment on the nonlinear absorption. To support this conclusion, the 2PA cross-section of TP-2Bzim was measured in glycerol. Remarkably, a particularly low value was determined (δ = 110 GM, λ_{exc} 840 nm) thereby confirming the crucial role of the DrewAT matrix that indeed induces a 10-fold enhancement of the 2PA ability of the dye. Notably, this enhancement was not observed previously in the TP-Py series for which the 2PA cross-sections were not significantly affected when passing from glycerol to DNA.[28] Likewise a low δ value (96 GM, λ_{exc} 840 nm) was found for TP-3bzim in glycerol confirming the influence of DNA but to a minor extent. Two important conclusions can be inferred from these observations: (i) In absence of DNA the TP-Bzim compounds show lower 2PA performances than the Py compounds (400−900 GM),[28] and the general quadrupole < octupole trend is not verified; and (ii) the two-photon absorption is switched-on by DNA, and this effect is especially spectacular for TP-2Bzim. Altogether these data are in line with conformational changes occurring upon DNA binding as suggested by the modeling studies.

It is known that the amplitude of the 2PA response in multibranched systems is influenced by the coupling between the dipolar arms and by the ground-state geometry of the individual arms.[36] Presumably, the tight immobilization of the dye inside the DNA matrix induces geometrical changes in both the ground and excited states compared to the structure of the free dye in solvent. Indeed the superposition of the structure of the free and bound dye shown in Figure 7 fully confirms this

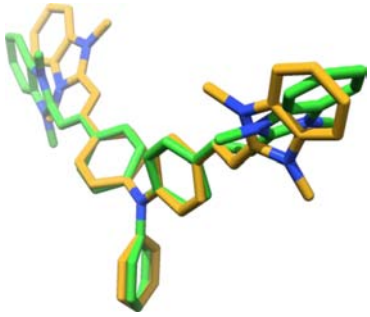

Figure 7. Modeling of TP-2Bzim: superposition of the docking pose in DrewAT (gold) and minimized structure without DNA (green).

hypothesis: It appears clearly that for the free dye, the Bzim motif is twisted with regard to the plane of the double bound obviously due to the steric hindrance of the two *N*-methyl groups, while the branch planarity is re-established for the bound dye. Thus TP-2Bzim is adopting a more flattened conformation upon "induced fit" in the minor-groove pocket, which results in an increased electronic conjugation in the branches. Altogether these conformational changes should enhance both the internal charge transfer in each branch and also the interarm coupling between the transition moments of the individual branches, thus causing a strong increase of the 2PA. This also explains why the fluorescence quantum yield of TP-2Bzim is further increased in DNA. All these effects are minimized or counterbalanced for TP-3Bzim due the third branch sticking out of the helix, thus retaining a lower conjugation and inducing higher molecular vibrations and stronger interactions with solvent.

This unprecedented and striking effect of the DNA matrix on the two photon absorption could not be evidenced with the TP-Py compounds due to the higher conjugation of the branches in the free state and a lower conformational modification upon binding to DNA. As well related 2PA probes possessing more rigid structures such as carbazoles, which have been explored by us and several other groups, show no strong 2PA sensitivity with respect to the DNA matrix.[40]

The measure of 2PA cross-section is subject to a strong dispersion depending mainly on the experimental conditions.[55] Consequently, we have also measured for comparison purposes the 2PA cross-section of Hoechst 33258 with the same experimental setup. Hoechst 33258 is a blue-emitting dye classically used for labeling nuclear DNA with excitation in UV or at 760 nm.[56] Remarkably, the two-photon cross-section of this dye is considerably lower (δ= 19GM) than that of TP-2Bzim (Table 2). If we compare now the dye performances in term of action cross-section ($\delta\times\Phi_F$), which is the relevant

dx.doi.org/10.1021/ja404422z | J. Am. Chem. Soc. 2013, 135, 12697−12706

figure of merit for imaging (also called molecular brightness), we find a spectacular enhancement of 83-fold for TP-2Bzim ($\delta \times \Phi_F$ = 583 vs 7 GM for Hoechst). This indicates that a considerably lower laser intensity can be applied when using TP-2Bzim, theoretically divided by a factor of 9 taken into account the quadratic dependendance of the 2PA absorption. Low to fair action cross-section values were obtained for the three other TP dyes, which fall in the range (10−50 GM) of most classical fluorophores used in biological imaging (fluorescein, DAPI, Cy3).[57]

These results emphasize the remarkable advantage brought by the TP-2Bzim scaffold to improve 2PA properties. Resulting from the concomitant optimization in quantum yield and in 2PA cross-section, the new dye TP-2bzim exhibits a remarkably elevated value of 2PA molecular brightness inside DNA yet unrivalled for a small-size molecule.[58]

Cellular Imaging of DNA with TP-2Bzim Dye. The TP-2Bzim dye was used to image DNA in a cellular context. Observations in confocal microscopy showed a bright and specific staining of nuclear DNA with excellent signal-to-noise ratio (Figure 8). Remarkably, the exceptional 2PA brightness of

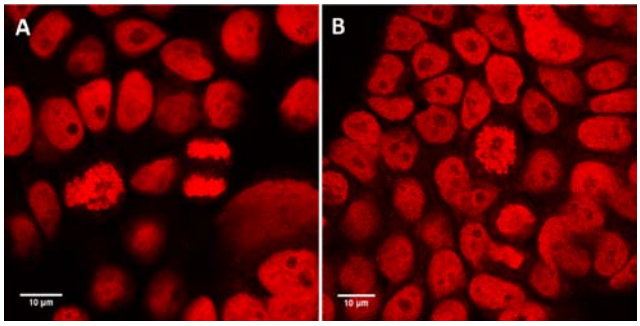

Figure 8. Confocal microscopy imaging of fixed HT29 cells incubated with TP-2Bzim at two different concentrations (A) 1 μM and (B) 100 nM under two-photon excitation (λ_{exc}: 800 nm). Light collected from 500 to 720 nm. Incubation made before PFA treatment of the cells.

TP-2Bzim allowed to image nuclear DNA in cells at very low dye loading (100 nM, Figure 8B) while keeping excitation light intensity at the level used for micromolar concentration (i.e., 10−30 MW/cm^2) (Figure 8A). Notably, although the TP-2Bzim has a somewhat blue-shifted fluorescence as compared to TP-Py, the emission can still be recorded in the red channel (600− 700 nm) while retaining a high sensitivity.

The absence of cytoplasmic and nucleoli labeling is very clear in consistency with the low binding to RNA shown *in vitro* (Figure 3). Such pattern showing dark nucleoli is a typical feature of DNA minor groove binders resulting of their strong specificity for B-helix duplexes over ssDNA and ssRNA.[50] Finally it is worth noting that two staining protocols were assayed: incubation on cells already fixed or incubation with live cells for 2 h before fixation. The same results were obtained thereby indicating that the dyes are cell permeant.

Because TP-2Bzim shows a pronounced AT sequence specificity, we were curious to verify if this property observed on a short oligonucleotide can be transposed for imaging at a macroscopic level in the context of chromatin. With this in mind we performed imaging of a cell line (3T3) known to contain AT-rich centromeric domains (Figure 9).

As seen in Figure 9 we observed bright spots that are typical of high dye density foci resulting from accumulation of TP-

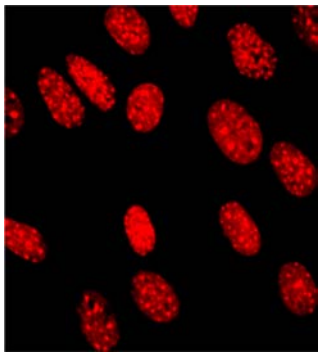

Figure 9. Labeling of mice fibroblasts (3T3) by TP-2Bzim. Foci represent AT-rich centromeres. Live cells were incubated with dye at a 1 μM concentration for 4 h, then washed several times with PBS buffer (1×), and fixed with paraformaldehyde (PFA); λ_{exc}: 488 nm.

2Bzim in the centromeric AT regions of 3T3 cells. Compounds that exploit the nature of the AT-rich DNA in nucleus are of particular interest for mapping AT stretches which are found in critical regions, such as replication origins, minisatellite centromeric regions, and provide binding sites for nuclear proteins.[59,60] Therefore detection of AT-rich regions is of particular importance to study phenomena involved in chromatin remodeling associated to senescence and tumorogenesis,[61] which opens perspectives toward further applications of TP-2Bzim.

Finally, like their parent TP-Py compounds, the TP-Bzim dyes show a remarkable photostability in cells under one- and two-photon excitation as shown in Figures 10 and S10. Indeed,

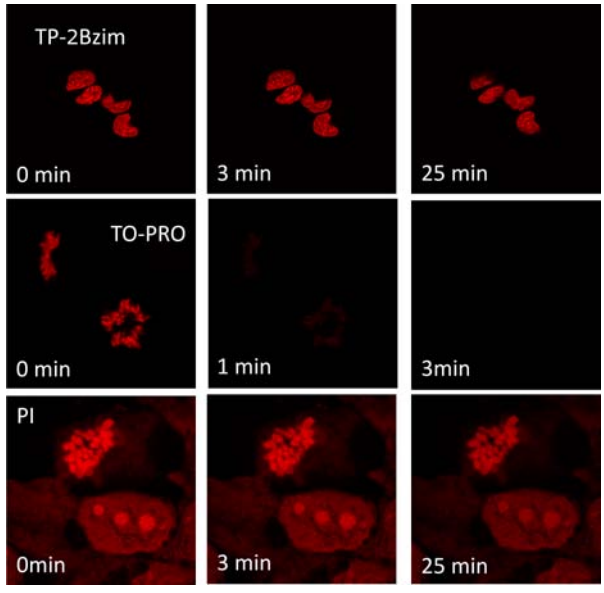

Figure 10. MRC-5 cells stained by TO-PRO-3 (2 μM, λ_{exc} =633 nm), PI (2 μM, λ_{exc} =561 nm), and TP-3Bzim (2 μM, λ_{exc} =488 nm) observed by confocal microscopy over a time lapse of 25 min.

for all TP-dyes, the fluorescence signal remains stable over a period of 30 min (Figure S10). For purpose of comparison the experiment was reproduced with the two commercially available red DNA stainers the cyanine TO-PRO3, and the PI derivative. The former faded in only 3 min (Figure 10), confirming its improper use for imaging. Only slight bleaching is observed with PI, but it accumulates strongly in the nucleoli

dx.doi.org/10.1021/ja404422z | J. Am. Chem. Soc. 2013, 135, 12697−12706

and also provides strong background in the cytoplasm (Figure 10). Thus, although widely used, PI requires ribonuclease (RNase) digestion before imaging and moreover is known to be cell impermeant. Consequently, the TP-2Bzim dye offers significant advantages over the commercial red DNA stainers: a RNase free staining protocol, an increased cell permeation, and a higher photostability under one- and two-photon excitation.

CONCLUSION

We obtained a new generation of vinyl triphenylamine-based dyes shaped for two-photon absorption by introducing two and three *N*-methyl benzimidazolium groups on the TP core which afforded the two derivatives TP-2Bzim and TP-3Bzim. These exhibit a bright orange-red light-up fluorescence in DNA and present huge fluorescence quantum yields (Φ_F = 0.34−0.54) which compare favorably with those of the best DNA stainers currently in use (SYBR green, Hoechst).[62] Molecular modeling indicates that the size and shape of the two-branch TP-2Bzim dye ensure a perfect geometric match with the minor groove of a 6AT tract resulting in a strong and selective fluorescence enhancement (140-fold) in AT-rich DNA. Unexpectedly the two-photon absorption of TP-2Bzim is dramatically increased (10-fold) in presence of DNA as compared to glycerol. This effect is attributed to a conformational switch induced by the DNA matrix, which modifies favorably the photophysics of the excited state and the geometry of the ground state thereby increasing the internal charge transfer favorable to the 2PA. This switch-on effect on two-photon absorption of dye inside a DNA matrix is unprecedented. As a consequence of improvement in quantum yield and in 2PA cross-section, TP-2Bzim bound to DNA is characterized by an exceptionally high two-photon brightness ($\delta\times\Phi_F$ = 583 GM). This enabled selective staining of nuclear DNA in fixed cells at submicromolar dye concentration. In addition the TP-2bzim dye was also shown to have substantial advantages as compared to the usual red DNA markers, such as a higher photostability, a better cell permeation, and a RNase-free staining protocol treatment. Finally, the AT-sequence preference of TP-2bzim was shown to afford AT-region specificity as revealed by imaging the AT-rich centromeric chromatin in 3T3 cells.

In summary, the new TP-2Bzim dye features a unique combination of optical and biological properties which makes it the molecule of choice for DNA staining as well as the best two-photon DNA-specific probe currently available. In particular its high photostability and fluorescence brightness per molecule are remarkable as these parameters remain prime figures of merit for virtually all ultrasensitive fluorescence spectroscopy and microscopy techniques. Ultimately, this new dye presents chemical versatility and scalability that are both desired for industrial development.

EXPERIMENTAL SECTION

Materials and Methods. *Chemical and Analyses.* All chemicals were purchased from Sigma-Aldrich (U.S.A.) or Acros Organics (Belgium) and used as received. All other chemicals were used as received from the appropriate suppliers. Preparative flash chromatographies were carried out with Merck silica gel (Si 60, 35−70 μm). NMR spectra were recorded on a Bruker Advance 300 spectrometer. ^{1}H NMR spectra were recorded at 300 MHz and ^{13}C NMR spectra at 75 MHz. Chemical shifts are reported in ppm downfield to TMS (δ = 0.00) for ^{1}H NMR and to central $CDCl_3$ resonance (δ = 77.16) or to [d_6]DMSO resonance (δ = 39.52) for ^{13}C NMR. High-performance liquid chromatography was carried out on a Waters Alliance equipped with a photodiode array detector using a XterraMS column with a linear gradient of acetonitrile versus water containing 0.1% of FA ranging from 10 to 55% over 5 min then to 100% over 6 min at a flow rate of 1 mL/min. Melting points were determined on a Kofler apparatus. Mass spectrometry was performed at the Institut Curie for Electrospray Ionization (ESI). High-resolution mass spectrometry was performed at the Institut de Chimie des Substances Naturelles (ICSN) in Gif-sur-Yvette. DAPI and PI were generous gifts from Marie Dutreix (Equipe recombinaison, réparation et cancer, Institut Curie). TO-PRO-3 was purchased from Molecular Probes, and Hoechst 33258 was purchased from Sigma-Aldrich. For all the tested compounds, stock solutions (from 1 to 10 mM depending on the compounds) were prepared in H_2O or in DMSO depending on the product solubility and kept at −18 °C.

Nucleic Acids and Oligonucleotides Sequences. MisTA (5′- GGG-TTA-CTA-CGA-ACT-GG-3′), ds26 (5′- CAA-TCG-GAT-CG A-ATT-CGA-TCC-GAT-TG-3′), and DrewAT (5′-CGCG-AAATTT-CGCG-3′) were purchased from Eurogentec (Belgium). The autocomplementary strands (DrewAT and ds26) were heated at 90 °C for 5 min in a 10 mM sodium cacodylate buffer pH 7.2, 100 mM NaCl (approximately duplex concentration 200 μM) and then slowly cooled to room temperature over 12 h. Once prepared, oligonucleotides solutions were stocked at 4 °C. Before use, the concentrations were evaluated by UV (after thermal denaturation 5 min at 90 °C) using the supplier's values for the molar extinction coefficients at 260 nm. Calf liver RNA was purchased from Sigma-Aldrich (U.S.A.). The lyophilized RNA was dissolved in 10 mM cacodylate buffer pH 7.2, 100 mM NaCl at a concentration of 5 mg·ml^{-1}. Concentration was checked by UV considering a molar absorption coefficient of 8700 M^{-1}·cm^{-1} at 260 nm (*Mol. Cell Biol.* **1977**, *18*, 81).

UV−vis Absorption, Fluorescence and CD Spectroscopies. Measurements were performed in 1 or 3 mL Hellma quartz cuvette (material code QS blue, 200−2000 nm). UV−vis experiments were monitored on a Uvikon XL (Secomam, France) UV spectrophotometer. Fluorescence spectra were recorded on a FluoroMax-3 (Jobin Yvon) at room temperature. Data were corrected with a blank and from the variations of the detector with the emitted wavelength. The CD spectra were recorded on a Jasco J-710 spectrometer thermostatted at 22 °C. Each spectrum is the accumulation of four scans performed with a 1 nm step and a 200 nm/min scanning speed. All experiments were performed in 10 mM sodium cacodylate buffer pH 7.2 prepared by dissolving sodium cacodylate trihydrate (Sigma-Aldrich, U.S.A.) in Milli-Q water.

Synthesis. *Synthesis of 2-(Chloromethyl)-1-methyl-1H-benzo[d]-imidazole* ***1****.* *N*1-methylbenzene-1,2-diamine (1g, 0.930 mL, 8.19 mmol) and 2-chloroacetic acid (1.160 g, 12.28 mmol, 1.5 equiv) were added in 2 N HCl. The resulting dark-purple solution is stirred at reflux overnight. After cooling at room temperature, the solution is brought to pH = 8 with NaOH 1 M and extracted twice with ethyl acetate. The combined organic phases are washed with brine dried over $MgSO_4$ and concentrated under reduced pressure. Raw product was purified by flash chromatography using Companion Combiflash automated apparatus (ethyl acetate/cyclohexane 50/50 to 80/20) to afford 1.116 g of the title compound as a white powder (75%). CAS number: 4760-35-4. ^{1}H NMR (300 MHz, chloroform-*d*) δ 7.77 (d, *J* = 7.2 Hz, 1H), 7.46−7.03 (m, 3H), 4.86 (s, 2H), 3.89 (s, 3H).

Synthesis of ((1-Methyl-1H-benzo[d]imidazol-2-yl)methyl)-triphenylphosphonium Chloride ***2****.* A solution of 2-(chloromethyl)-1-methyl-1H-benzo[*d*]imidazole (883 mg, 4.89 mmol) and triphenylphosphine (1.923 g, 7.33 mmol, 1.5 equiv) in 15 mL toluene was heated at reflux. A white precipitate forms. After one night of stirring, the precipitates are filtered under reduced pressure, washed with pentane, and dried under reduced pressure to afford 1.206 g of the expected product as a white solid (56%). CAS number: 68426-76-6. ^{1}H NMR (300 MHz, chloroform-*d*) δ 7.96 (dd, *J* = 13.0, 7.8 Hz, 6H), 7.75 (t, *J* = 7.2 Hz, 3H), 7.69−7.53 (m, 6H), 7.47 (d, *J* = 7.8 Hz, 1H), 7.32−7.08 (m, 3H), 6.03 (d, *J* = 14.8 Hz, 2H), 3.93 (s, 3H).

Synthesis of 4-((E)-2-(1-methyl-1H-benzo[d]imidazol-2-yl)vinyl)-N-(4-((E)-2-(1-methyl-1H-benzo[d]imidazol-2-yl)vinyl)phenyl)-N-phenylaniline ***4a****.* To a solution of 4,4′-bisformyltriphenylamine (50 mg, 0.166 mmol) and **2** (162 mg, 0.365 mmol, 2.2 equiv) in 5 mL

methanol is added 5 mL of a freshly prepared solution of sodium methanolate in methanol (19 mg Na, 0.830 mmol, 5 equiv). After one night of stirring, the solution is left to cool at room temperature and concentrated under reduced pressure. The residue is dissolved in DCM. Pentane is added until precipitation of a yellow solid. The precipitate is filtered under reduced pressure, washed with pentane, and dried under vacuum to afford 79 mg of the title compound (85%). mp °C: 150−152; ^{1}H NMR (300 MHz, chloroform-*d*) δ 7.93 (d, J = 15.8 Hz, 2H), 7.83−7.69 (m, 2H), 7.52 (d, J = 8.3 Hz, 4H), 7.43−7.23 (m, 8H), 7.21−7.15 (m, 2H), 7.12 (d, J = 8.2 Hz, 4H), 7.00 (d, J = 15.8 Hz, 2H), 3.87 (s, 3H). ^{13}C NMR (75 MHz, $CDCl_3$) δ 151.56, 148.22, 146.86, 143.29, 136.90, 136.18, 130.68, 129.76, 128.53, 125.76, 124.46, 123.80, 122.77, 122.58, 119.33, 111.27, 109.23, 29.93. HRMS (ESI+): m/z calcd for $[C_{38}H_{31}N_5]^+$, 558.2658; found, 558.2657

Synthesis of Tris(4-((E)-2-(1-methyl-1H-benzo[d]imidazol-2-yl)-vinyl)phenyl)amine ***4b****.* According to the same procedure, 200 mg of 4,4′,4″-triformyltriphenylamine (0.607 mmol) led to 282 mg of the title compound as a yellow solid (65%). mp °C: 192−194; ^{1}H NMR (300 MHz, chloroform-*d*) δ 7.95 (d, J = 15.6 Hz, 3H), 7.85−7.66 (m, 3H), 7.55 (d, J = 7.7 Hz, 6H), 7.40−7.22 (m, 9H), 7.17 (d, J = 7.6 Hz, 6H), 7.03 (d, J = 15.8 Hz, 3H), 3.87 (s, 9H). ^{13}C NMR (75 MHz, $CDCl_3$) δ 151.3, 147.5, 143.1, 136.5, 136.0, 131.3, 128.5, 124.4, 122.6, 122.5, 119.1, 111.6, 109.1, 29.8. HRMS (ESI+): m/z calcd for $[C_{48}H_{39}N_7]^+$, 740.3345; found, 740.3373.

Synthesis of 2,2′-((1E,1′E)-((phenylazanediyl)bis(4,1-phenylene))-bis(ethene-2,1-diyl))bis(1,3-dimethyl-1H-benzo[d]imidazol-3-ium) Iodide TP-2Bzim. To a solution of **4a** (48 mg, 0.086 mmol) in 2 mL dichloromethane and 2 mL methanol is added a large excess of methyl iodide (1 mL). The solution turns red. After stirring overnight at 40 °C, pentane is added until a red precipitates forms. The solid is filtered under reduced pressure, washed with pentane, and dried under vacuum to afford 40 mg of the pure product (55%). ^{1}H NMR (300 MHz, DMSO-d_6) δ 8.05 (dd, J = 6.0, 2.9 Hz, 4H), 7.90 (d, J = 8.4 Hz, 4H), 7.79 (d, J = 16.8 Hz, 2H), 7.70 (dd, J = 6.2, 2.9 Hz, 4H), 7.53−7.36 (m, 4H), 7.34−7.23 (m, 1H), 7.23−7.13 (m, 6H), 4.14 (s, 12H). ^{13}C NMR (75 MHz, DMSO-d_6) δ 149.0, 148.6, 145.8, 145.7, 132.0, 130.3, 129.0, 126.4, 126.1, 125.5, 123.0, 112.9, 105.9, 33.0. HRMS (ESI+): m/z calcd for $[C_{40}H_{37}N_5]^{2+}$, 293.6525; found, 293.6520.

Synthesis of 2,2′,2″-((1E,1′E,1″E)-(nitrilotris(benzene-4,1-diyl))tris-(ethene-2,1-diyl))tris(1,3-dimethyl-1H-benzo[d]imidazol-3-ium) Iodide TP-3Bzim. According to the same procedure, 40 mg of **4b** (0.056 mmol) led to 55 mg of the pure compound as a red solid (86%). ^{1}H NMR (300 MHz, DMSO-d_6) δ 8.07 (dd, J = 6.2, 3.1 Hz, 6H), 7.99 (d, J = 8.4 Hz, 6H), 7.84 (d, J = 16.7 Hz, 3H), 7.71 (dd, J = 6.2, 3.0 Hz, 6H), 7.51 (d, J = 16.7 Hz, 3H), 7.28 (d, J = 8.0 Hz, 6H), 4.16 (s, 18H). HRMS (ESI+): m/z calcd for $[C_{51}H_{48}N_7]^{3+}$, 252.7990; found, 253.1304.

Two-Photon Absorption Cross-Section Measurements. Two-photon induced fluorescence measurements were performed at the CEA (Saclay) using an inverted microscope setup coupled to a mode locked Ti-sapphire laser (Tsunami, Spectra Physics) delivering 100 fs pulses with a 76 MHz repetition rate over the spectral range covering 740−950 nm. The Ti-sapphire excitation beam was focused in a cell filled with low-concentration solutions using a 40× microscope objective, the same objective being also used for the two-photon fluorescence signal collection. The signal is then sent either to a channel plate multiplier (Perkin-Elmer MP-993-CL) or to a spectrometer coupled to a CCD camera (Andor DU401-BR-DD) for detailed study of the emission spectra. The laser beam was linearly polarized, and a set of half-wave plate and polarizer was used to vary the fundamental beam intensity (700 μW at the level of the sample). Excitation spectra were determined from measurements of the whole emitted light using a photomultiplier proceeded with filters cutting the fundamental beam (SemRock razor edge 785, stopline 785 and 808, FF735 and FF-01-750). The TPIF intensities of the samples were measured relative to a solution of fluorescein in water (pH = 13), the ratio of the fluorescent signals enabling further determination of the 2PA cross-section (δ) assuming equal one- and two-photon fluorescence quantum yields.

Molecular Modeling. Ligand drawing, standardization (protonation state at physiological pH, aromatization, hydrogen treatment), and 3D generation were done with Chemaxon Marvin Beans. Docking was performed with the Surflex-Dock engine of the Tripos SYBYL-X 2.0 suite. The modified GeomX mode was used throughout the calculations with the option Allow DNA movement: six additional starting conformations were generated, pre- and postdock minimizations were performed, a maximum of three final poses were saved, with a minimum of 0.5 RMSD between poses. The spin alignment method was used, with an exhaustive accuracy (density of search 9.0) and 12 number of spins per alignment. A DrewAT-like structure was built using SYBYL-X 2.0 (biopolymer builder module), and the binding site centered on the central AATT sequence was determined by protomol probes (CH_4 as a steric hydrophobic probe, NH as a H-bond donor probe, C═O as a H-bond acceptor probe). The docking results are ranked based on an empirical scoring function including hydrophobic, polar, repulsive, entropic, solvation, and crash terms and expressed in $-\log_{10}(K_d)$ units to represent binding affinities.

The minimized conformation of TP-2Bzim was found using the genetic algorithm-based global optimizer in Sybyl-X 2.0 with the default parameters.

Cell Culture and Fluorescence Microscopy. Cells were grown on coverslips at 37 °C in monolayer cultures in complete DMEM (Gibco, Cergy Pontoise, France) with 10% FCS and antibiotics (100 mg/mL streptomycin and 100 mg/mL penicillin) under conditions of 100% humidity, 95% air, and 5% CO2 for 24 h. The cells were then incubated for 2 h with the compounds (concentration indicated in the text). After washing twice with PBS, the cells were fixed with 4% paraformaldehyde and washed with PBS twice. The coverslips were then mounted on microscope slides using Prolong Gold antifade reagent (Invitrogen).

The confocal and biphotonic imaging was performed using a confocal laser scanning microscope DMI 6000 with a SP5-AOBS unit (both Leica) equipped with a 63× (NA = 1.4) objective (oil immersion), an argon gas laser for one-photon excitation, and a Chameleon Ti:sapphire laser delivering pulses in the 100−200 fs range at an 80 MHz repetition rate with a tunability ranging from 705 to 980 nm for two-photon excitation.

■ ASSOCIATED CONTENT

Ⓢ Supporting Information

Detailed methods for fluorescence quantum yield measurement and nonlinear curve analysis and ddditional figures and tables. This material is available free of charge via the Internet at http://pubs.acs.org.

■ AUTHOR INFORMATION

Corresponding Author

mp.teulade-fichou@curie.fr

Present Address

[§]Université P. Sabatier, Lab IMRCP, CNRS UMR 5623, Bât 2R1, 118 route de Narbonne, 31062 Toulouse cedex 09 France.

Author Contributions

[‖]These authors contributed equally.

Notes

The authors declare no competing financial interest.

■ ACKNOWLEDGMENTS

ANR-07-PCVI-0005−01 (EPATAN) and NanoBioIdf (Label DNA) are acknowledged for fundings and in particular for post doctoral and Ph.D. fellowship to E.F.-P. and G.M. The authors wish to thank Drs. Maria Quanz, Nathalie Gagey, and Florent Poyer for their help in microscopy imaging and cell culture.

REFERENCES

(1) Sinkeldam, R. W.; Greco, N. J.; Tor, Y. *Chem. Rev.* **2010**, *110*, 2579−619.
(2) Wysocki, L. M.; Lavis, L. D. *Curr. Opin. Chem. Biol.* **2011**, *15*, 752−9.
(3) Cassette, E.; Helle, M.; Bezdetnaya, L.; Marchal, F.; Dubertret, B.; Pons, T. *Adv. Drug Delivery Rev.* **2013**, *65*, 719−731.
(4) Giepmans, B. N. G.; Adams, S. R.; Ellisman, M. H.; Tsien, R. Y. *Science* **2006**, *312*, 217−24.
(5) Ishikawa-Ankerhold, H. C.; Ankerhold, R.; Drummen, G. P. C. *Molecules* **2012**, *17*, 4047−132.
(6) Fernández-Suárez, M.; Ting, A. Y. *Nat. Rev. Mol. Cell Biol.* **2008**, *9*, 929−43.
(7) Flors, C.; Earnshaw, W. C. *Curr. Opin. Chem. Biol.* **2011**, *15*, 838−44.
(8) Zipfel, W. R.; Williams, R. M.; Webb, W. W. *Nat. Biotechnol.* **2003**, *21*, 1369−77.
(9) Denk, W.; Strickler, J.; Webb, W. *Science* **1990**, *248*, 73−76.
(10) Oheim, M.; Michael, D. J.; Geisbauer, M.; Madsen, D.; Chow, R. H. *Adv. Drug Delivery Rev.* **2006**, *58*, 788−808.
(11) Morales, A. R.; Yanez, C. O.; Zhang, Y.; Wang, X.; Biswas, S.; Urakami, T.; Komatsu, M.; Belfield, K. D. *Biomaterials* **2012**, *33*, 8477−85.
(12) Andrade, C. D.; Yanez, C. O.; Ahn, H.-Y.; Urakami, T.; Bondar, M. V; Komatsu, M.; Belfield, K. D. *Bioconj. Chem.* **2011**, *22*, 2060−71.
(13) Kim, H. M.; Cho, B. R. *Acc. Chem. Res.* **2009**, *42*, 863−72.
(14) Wang, B.-G.; König, K.; Halbhuber, K.-J. *J. Microsc.* **2010**, *238*, 1−20.
(15) Choong, F. X.; Sandoval, R. M.; Molitoris, B. A.; Richter-Dahlfors, A. *Meth. Enzymol.* **2012**, *506*, 35−61.
(16) Kowada, T.; Kikuta, J.; Kubo, A.; Ishii, M.; Maeda, H.; Mizukami, S.; Kikuchi, K. *J. Am. Chem. Soc.* **2011**, *133*, 17772−6.
(17) Hopt, A.; Neher, E. *Biophys. J.* **2001**, *80*, 2029−36.
(18) Pawlicki, M.; Collins, H. A.; Denning, R. G.; Anderson, H. L. *Angew. Chem., Int. Ed.* **2009**, *48*, 3244−66.
(19) D'Aléo, A.; Bourdolle, A.; Brustlein, S.; Fauquier, T.; Grichine, A.; Duperray, A.; Baldeck, P. L.; Andraud, C.; Brasselet, S.; Maury, O. *Angew. Chem., Int. Ed.* **2012**, *51*, 6622−5.
(20) Lim, C. S.; Masanta, G.; Kim, H. J.; Han, J. H.; Kim, H. M.; Cho, B. R. *J. Am. Chem. Soc.* **2011**, *133*, 11132−5.
(21) Morales, A. R.; Yanez, C. O.; Schafer-hales, K. J.; Marcus, A. I.; Belfield, K. D. *Bioconj. Chem.* **2009**, *20*, 1992−2000.
(22) Belfield, K. D.; Bondar, M. V; Morales, A. R.; Yue, X.; Luchita, G.; Przhonska, O. V *J. Phys. Chem. C* **2012**, *116*, 11261−11271.
(23) Xu, C.; Webb, W. W. *J. Opt. Soc. Am. B* **1996**, *13*, 481−491.
(24) Xu, C.; Zipfel, W.; Shear, J. B.; Williams, R. M.; Webb, W. W. *Proc. Natl. Acad. Sci. U.S.A.* **1996**, *93*, 10763−8.
(25) Granzhan, A.; Teulade-Fichou, M.-P. *Chem.—Eur. J.* **2009**, *15*, 1314−8.
(26) Largy, E.; Granzhan, A.; Hamon, F.; Verga, D.; Teulade-Fichou, M.-P. *Top. Curr. Chem.* **2013**, *330*, 111−77.
(27) Yang, P.; De Cian, A.; Teulade-Fichou, M.-P.; Mergny, J.-L.; Monchaud, D. *Angew. Chem., Int. Ed.* **2009**, *48*, 2188−91.
(28) Allain, C.; Schmidt, F.; Lartia, R.; Bordeau, G.; Fiorini-Debuisschert, C.; Charra, F.; Tauc, P.; Teulade-Fichou, M.-P. *ChemBioChem* **2007**, *8*, 424−433.
(29) Dumat, B.; Bordeau, G.; Aranda, A. I.; Mahuteau-Betzer, F.; El Harfouch, Y.; Metgé, G.; Charra, F.; Fiorini-Debuisschert, C.; Teulade-Fichou, M.-P. *Org. Biomol. Chem.* **2012**, *10*, 6054−61.
(30) Katan, C.; Terenziani, F.; Mongin, O.; Werts, M. H. V; Porrès, L.; Pons, T.; Mertz, J.; Tretiak, S.; Blanchard-Desce, M. *J. Phys. Chem. A* **2005**, *109*, 3024−37.
(31) Chung, S.-J.; Kim, K.-S.; Lin, T.-C.; He, G. S.; Swiatkiewicz, J.; Prasad, P. N. *J. Phys. Chem. B* **1999**, *103*, 10741−10745.
(32) Lambert, C.; Gaschler, W.; Schmälzlin, E.; Meerholz, K.; Bräuchle, C. *J. Chem. Soc., Perkin Trans. 2* **1999**, 577−588.
(33) Bellmann, E.; Shaheen, S. *Chem. Mater.* **1998**, *4756*, 1668−1676.
(34) Roquet, S.; Cravino, A.; Leriche, P.; Alévêque, O.; Frère, P.; Roncali, J. *J. Am. Chem. Soc.* **2006**, *128*, 3459−66.
(35) Zyss, J.; Ledoux, I. *Chem. Rev.* **1994**, *94*, 77−105.
(36) Beljonne, D.; Wenseleers, W. *Adv. Funct. Mater.* **2002**, *12*, 631−641.
(37) Bordeau, G.; Lartia, R.; Metge, G.; Fiorini-Debuisschert, C.; Charra, F.; Teulade-Fichou, M.-P. *J. Am. Chem. Soc.* **2008**, *130*, 16836−7.
(38) Bhaskar, A.; Ramakrishna, G.; Lu, Z.; Twieg, R.; Hales, J. M.; Hagan, D. J.; Van Stryland, E.; Goodson, T. *J. Am. Chem. Soc.* **2006**, *128*, 11840−11849.
(39) Lartia, R.; Allain, C.; Bordeau, G.; Schmidt, F.; Fiorini-Debuisschert, C.; Charra, F.; Teulade-Fichou, M.-P. *J. Org. Chem.* **2008**, *73*, 1732−1744.
(40) Dumat, B.; Bordeau, G.; Faurel-Paul, E.; Mahuteau-Betzer, F.; Saettel, N.; Bombled, M.; Metgé, G.; Charra, F.; Fiorini-Debuisschert, C.; Teulade-Fichou, M.-P. *Biochimie* **2011**, *93*, 1209−1218.
(41) Wolter, F. E.; Schneider, K.; Davies, B. P.; Socher, E. R.; Nicholson, G.; Seitz, O.; Süssmuth, R. D. *Org. Lett.* **2009**, *11*, 2804−7.
(42) Monchaud, D.; Allain, C.; Bertrand, H.; Smargiasso, N.; Rosu, F.; Gabelica, V.; De Cian, A.; Mergny, J.-L.; Teulade-Fichou, M.-P. *Biochimie* **2008**, *90*, 1207−23.
(43) Neidle, S. *Nat. Prod. Rep.* **2001**, *18*, 291−309.
(44) Bailly, C.; Chaires, J. B. *Bioconj. Chem.* **1998**, *9*, 513−38.
(45) Boykin, D. W.; Tidwell, R. R. In *DNA and RNA binders*; Demeunynck, M.; Bailly, C.; Wilson, W. D., Eds.; Weinheim, 2003; pp 414−460.
(46) Eriksson, M.; Nordén, B. In *Methods in Enzymology*; Chaires, J. B.; Waring, M. J., Eds.; Academic Press: New York, 2001; Vol. *340*, pp 68−98.
(47) Tanious, F. A.; Ding, D.; Patrick, D. A.; Bailly, C.; Tidwell, R. R.; Wilson, W. D. *Biochemistry* **2000**, *39*, 12091−101.
(48) Seifert, J.; Connor, R.; Kushon, S. A.; Wang, M.; Armitage, B. A. *J. Am. Chem. Soc.* **1999**, 2987−2995.
(49) Mazur, S.; Tanious, F. a; Ding, D.; Kumar, a; Boykin, D. W.; Simpson, I. J.; Neidle, S.; Wilson, W. D. *J. Mol. Biol.* **2000**, *300*, 321−37.
(50) Spitzer, G. M.; Fuchs, J. E.; Markt, P.; Kirchmair, J.; Wellenzohn, B.; Langer, T.; Liedl, K. R. *Chemphyschem* **2008**, *9*, 2766−71.
(51) Liu, Y.; Kumar, A.; Depauw, S.; Nhili, R.; David-Cordonnier, M.-H.; Lee, M. P.; Ismail, M. A.; Farahat, A. A.; Say, M.; Chackal-Catoen, S.; Batista-Parra, A.; Neidle, S.; Boykin, D. W.; Wilson, W. D. *J. Am. Chem. Soc.* **2011**, *133*, 10171−10183.
(52) Nguyen, B.; Neidle, S.; Wilson, W. D. *Acc. Chem. Res.* **2009**, *42*, 11−21.
(53) Shaikh, S. A.; Ahmed, S. R.; Jayaram, B. *Arch. Biochem. Biophys.* **2004**, *429*, 81−99.
(54) Porrès, L.; Mongin, O.; Katan, C.; Charlot, M.; Pons, T.; Mertz, J.; Blanchard-Desce, M. *Org. Lett.* **2004**, *6*, 47−50.
(55) Chandra Jha, P.; Wang, Y.; Agren, H. *ChemPhysChem* **2008**, *9*, 111−6.
(56) Martin, R. M.; Leonhardt, H.; Cardoso, M. C. *Cytometry, Part A* **2005**, *67*, 45−52.
(57) Lukomska, J.; Gryczynski, I.; Malicka, J.; Makowiec, S.; Lakowicz, J. R.; Gryczynski, Z. *Biochem. Biophys. Res. Commun.* **2005**, *328*, 78−84.
(58) Yao, S.; Belfield, K. D. *Eur. J. Org. Chem.* **2012**, *2012*, 3199−3217.
(59) Woynarowski, J. M. *Biochim. Biophys. Acta* **2002**, *1587*, 300−8.
(60) Reeves, R. *Gene* **2001**, *277*, 63−81.
(61) Narita, M.; Narita, M.; Krizhanovsky, V.; Nuñez, S.; Chicas, A.; Hearn, S. a; Myers, M. P.; Lowe, S. W. *Cell* **2006**, *126*, 503−14.
(62) Cosa, G.; Focsaneanu, K. S.; McLean, J. R.; McNamee, J. P.; Scaiano, J. C. *Photochem. Photobiol.* **2001**, *73*, 585−99.